Available online at www.sciencedirect.com

SciVerse ScienceDirect

Ceramics International 39 (2013) 5241–5246

CERAMICS INTERNATIONAL

www.elsevier.com/locate/ceramint

Electrical, structural and thermal properties of nanoceramic $(Bi_2O_3)_{1-x-y}(Ho_2O_3)_x(Tm_2O_3)_y$ ternary system

S. Durmuş[a,*], V. Çorumlu[b], T. Çifci[b], I. Ermis[b], M. Arı[c]

[a]Department of Energy Systems Engineering, Faculty of Technology, Dumlupınar University, 43500 Kütahya, Turkey
[b]Institute of Science, Erciyes University, 38039 Kayseri, Turkey
[c]Department of Physics, Faculty of Sciences, Erciyes University, 38039 Kayseri, Turkey

Received 13 September 2012; received in revised form 7 December 2012; accepted 8 December 2012
Available online 28 December 2012

Abstract

Ho_2O_3 and Tm_2O_3 doped Bi_2O_3 composite electrolyte type materials for solid oxide fuel cells (SOFCs) operating at intermediate-temperature were investigated. The bismuth-based ceramic powders were produced by using conventional solid-state synthesis techniques. The products were characterized by means of scanning electron microscopy (SEM), X-ray powder diffraction (XRD), differential thermal analysis/thermal gravimetry (DTA/TG), and the four-point probe technique (4PPT). XRD and DTA/TG measurements indicate that all of the samples have the stable fluorite type face centered cubic (fcc) δ-phase. 4PPT measurements were performed in the temperature range 150–1000 °C in air and these measurements showed that the electrical conductivity of the samples decrease with increasing amount of Tm_2O_3. This increase in the electrical conductivity of the samples could be attributed to the increase in the numbers of highly polarizable cations and oxide ion vacancies. The highest conductivity value was found as $5.31 \times 10^{-1}\ \Omega\ cm^{-1}$ for the $(Bi_2O_3)_{1-x-y}(Ho_2O_3)_x(Tm_2O_3)_y$ ternary system (for $x=20$ and $y=5$ mol%) at 1000 °C. The activation energies of the samples were calculated from log σ graphics versus $1000/T$. These calculated results showed that the translation motion of the charge carriers, oxygen vacancies, and space charge polarizations are responsible for the change in activation energy as a function of temperature.

Keywords: Solid oxide fuel cell (SOFC); Ceramic electrolyte; X-ray diffraction; 4-point probe technique

1. Introduction

Solid oxide fuel cells (SOFCs) are very efficient electrochemical energy-conversion systems because of their high energy conversion efficiency, high power density, clean and environmentally friendly output when hydrogen is used as fuel, and flexibility in using various fuels [1].A conventional high temperature-SOFC (HT-SOFC) based on yttria-stabilized zirconia (YSZ) electrolyte operates at a high temperature range of 800–1000 °C. This high operation temperature causes an increase in the cost price of the system and unwanted chemical reactions and mismatch problems between the components of the SOFC, and the special materials for isolation and interconnectors to be used in the construction of the SOFC. When the operation temperature of SOFCs is decreased to a lower temperature range for example 600–800 °C, it is possible to get rid of many unwanted problems and obtain some advantages, such as a significant reduction in production and application costs, choice of different electrolyte materials and other components such as metal interconnectors which improve the overall stability, reliability, and performance of SOFCs [2–5].

In recent years, Bi_2O_3-based materials have been considered as potential materials for solid oxide fuel cell electrolyte due to their high oxygen ionic conductivity. They have also been shown to be the most promising electrolytes for intermediate operating temperatures (600–800 °C) of SOFCs since they have higher oxygen ion conductivity compared with other materials with similar properties [6–8]. In addition, Bi_2O_3-based materials are used in many industrial productions, such

*Corresponding author. Tel.: +90 54 2639 2669.
E-mail address: semradurmus38@hotmail.com (S. Durmuş).

0272-8842/$ - see front matter © 2012 Elsevier Ltd and Techna Group S.r.l. All rights reserved.
http://dx.doi.org/10.1016/j.ceramint.2012.12.024

as oxygen sensors, oxygen separation membranes, oxygen pumps, catalyzing reactions, for the oxidation of hydrocarbons and as additive material in paints [9–11]. Many researchers have focused on the properties of oxide doped Bi_2O_3-based electrolytes operating at intermediate temperatures and most of them have attempted to overcome the instability problems of the materials to obtain better performance in technological applications [6–9,12]. Therefore, different types of bismuth oxide-based electrolyte materials with stable structure and high ionic conductivity need to be developed for the SOFC applications. Researchers have carried out many studies to synthesize single oxide-doped Bi_2O_3-based materials which have high ionic conductivity at intermediate temperature but lack of structural stability [13–15]. Also, double-layer electrolyte concept has been developed to overcome thermodynamically instability of δ-phase Bi_2O_3 [14–19]. Recently, in the literature, some works [14–20] showed that the ionic conductivity of the double-doped systems has been found to be better than the ionic conductivity of the single-doped systems.

The δ-phase is one of the six known phases of Bi_2O_3 (α, β, γ, δ, ε, and ω) [21]. It is stable only in the temperature range 730–825 °C [22]. However, by the addition of appropriate dopants, such as rare-earth material oxides or many other oxides [23,24], the δ-phase can be stabilized and prevented even at room temperature [25].

In this work, we synthesized holmium oxide (Ho_2O_3) and thulium oxide (Tm_2O_3) doped Bi_2O_3 nanoceramic powders by the solid state reaction method for obtaining the stable δ-phase materials which can be used as an electrolyte material in SOFCs. The morphological, structural, thermal and electrical properties of the synthesized materials were investigated by using the SEM, XRD, DTA/TG, and 4PPT.

2. Experimental procedures

2.1. Sample preparation

In order to synthesize the samples, bismuth(III) oxide (99·99%, Alfa Asear), holmium(III) oxide (99·99%, Alfa Asear) and thulium(III) oxide (99·99%, Alfa Asear) were used as starting materials. Eight different compositions of the ceramic oxide mixtures were prepared with $x=15$, 20 mol% and $y=5$, 10, 15, 20 mol% of the stoichiometric amounts in the $(Bi_2O_3)_{1-x-y}(Ho_2O_3)_x(Tm_2O_3)_y$ ternary system. The electrolyte samples were prepared in two steps. First, the desired proportion of each of the starting materials (Bi_2O_3, Ho_2O_3, Tm_2O_3) was accurately weighed and then they were thoroughly mixed by grinding in an agate mortar. Then, an amount of each mixture powder (2 g) was heated in an alumina crucible at 750 °C for 100 h to obtain stable fluorite type face-centered cubic (fcc) δ-phase electrolyte samples. We used these prepared mixtures in the XRD and DTA/TG measurements. The rest of each mixture (1.5 g) was pressed in a die of 13 mm diameter under pressure (10 t/cm^2) to obtain a disk shaped pellet and these pellets were sintered for a second time at 750 °C for 100 h in air to obtain long term phase stability. All of the solid state reactions were performed using loose powders, in alumina crucibles, in an air atmosphere and without any compaction. We used these pellets in the SEM and 4PPT measurements.

2.2. Structural and thermal measurements

The XRD measurements were carried out by using a Bruker AXS D8 Advance type diffractometer with an interval $2\theta=10°$–$90°$, scanning 0.002°/min, and Cu-K_α radiation for the determination of the crystal structure of the samples at room temperature. Then, the DiffracPlus Eva-TOPAS 2 and WinIndex softwares were used to determine the crystal structures, unit lattice cell parameters (a, b, c, α, β, γ), Miller indexes, and the distance, d, between the layers.

The composite morphology of the samples was taken by scanning electron microscopy (Leo 440 Computer Controlled Digital) on samples sputtered with gold and observed at an accelerating voltage of 10 kV.

The thermal behavior of the annealed materials was investigated by TG/DTA by means of the Diamond TG/DTA-Perkin Almer Marck system. About 20–50 mg of the sample powder was heated at 200 °C min^{-1} in an alumina crucible and cooled to room temperature during the measurement under a stream of air.

2.3. Electrical measurements

The electrical conductivity measurements were carried out by using the 4PPT on the powder materials which were pressed into a disk shaped pellet. The measuring unit was interfaced with a PC for on-line data acquisition and processing. A Keithley 2400 sourcemeter was used to provide a constant current and the potential drop was detected by a Keithley 2700 multimeter with a 7700 data logging card. Pt wires with a diameter of 0.5 mm were employed as current and potential probes. Electrical resistivity and conductivity were determined from the detected current and voltage drop using a standard conversion method. The temperature of the sample was changed by a controllable Nabertherm furnace. The temperature of the samples was also measured using a0.5 mm standard K type thermocouple which was placed very close to the sample and detected with the Keithley 2700 multimeter. By using the 4PPT, the measurement errors due to wire resistance, the spreading resistance under each wire, and the contact resistances between each metal wire and the samples were eliminated.

3. Results and discussions

3.1. Structural analysis

In order to see the symmetry of the crystal structure and any phase changes, the XRD patterns of all samples of

$(Bi_2O_3)_{1-x-y}(Ho_2O_3)_x(Tm_2O_3)_y$ system given in Fig. 1. As seen from Fig. 1, these XRD patterns show that the crystal structure of this sample belongs to a fluorite type fcc symmetry of the δ-phase Bi_2O_3. During the electrical conductivity measurements, additional heat treatment was applied to samples by a heating/cooling cycle and there is no phase change even after electrical measurement.

The fcc δ-phase structure clearly appeared and according to the ICDD Grant-in-Aid primary reference, it corresponds to a typical XRD spectrum of holmium stabilized δ-phase Bi_2O_3 for the calcined powder. The reflection peaks appearing at $2\theta=28.06^\circ$ (1 1 1), 32.53° (2 0 0), 46.71° (2 2 0), 55.44° (3 1 1), 58.03° (2 2 2), 68.19° (4 0 0), 75.30° (3 3 1), 77.62° (4 2 0), and 86.70° (4 2 2) are in a good agreement with results from the powder diffraction file (PDF). The unit cell parameters of the samples were determined by using WinIndex software. The unit cell parameter decreases with increasing the doping amount of Tm_2O_3. The results were given in Table 1.

The XRD patterns were also taken from finely ground powder; these mostly had submicron sized grains. The average particle sizes of the δ-phase type samples were also determined by using XRD peak data in Scherrer–Warren equations:

$$D = 0.9\lambda/(B\cos\theta_B) \quad (1)$$

where λ is the wavelength of the X-ray, D is the average crystallite size, θ_B is the Bragg diffraction angle of the considered XRD peaks, and B represents the fwhm line broadening obtained as follows:

$$B^2 = B^2{}_m - B^2{}_s \quad (2)$$

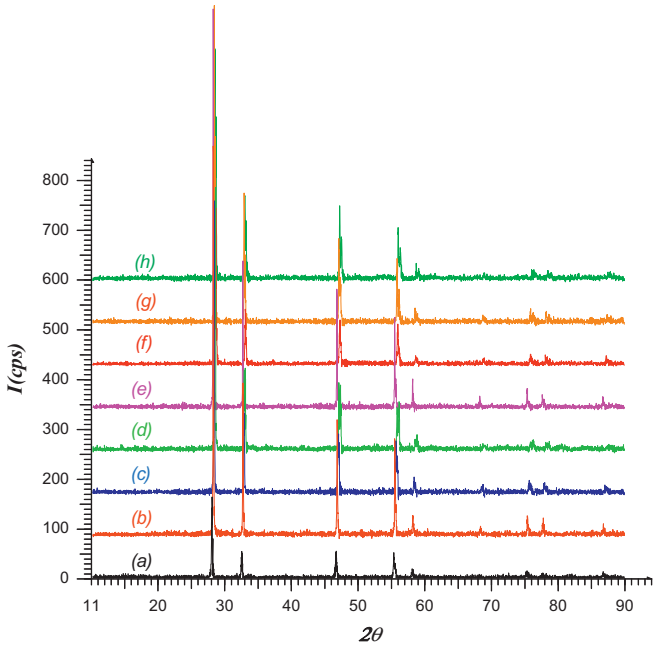

Fig. 1. The XRD patterns of all samples of $(Bi_2O_3)_{1-x-y}(Ho_2O_3)_x(Tm_2O_3)_y$ ternary system.

where B_m is the corrected half width which is obtained from the observed half width of the selected XRD peaks and B_s represents the half width of the reflections in the internal standard sample. In this study, the resulting values of the crystallite sizes obtained by using a Bruker AXS D8 the DiffracPlus Eva-TOPAS 2 from the strongest diffraction peaks that belong to the crystal planes of (1 1 1), (2 0 0), (2 2 0) and (3 1 1) are given in Table 1.

Fig. 2 shows the variation of the crystallite sizes of the materials (15 and 20% Ho_2O_3) as a function of the amount of Tm_2O_3 (5, 10, 15, 20%). As seen from Fig. 2, the crystallite sizes of both of these materials decrease with the increasing amount of Tm_2O_3 and they become equal to each other for 20 mol% of Tm_2O_3.

The SEM micrographs of the samples, (a) $(Bi_2O_3)_{0.80}(Ho_2O_3)_{0.15}(Tm_2O_3)_{0.05}$ and (b) $(Bi_2O_3)_{0.75}(Ho_2O_3)_{0.20}(Tm_2O_3)_{0.05}$ are shown in Fig. 3a and b, respectively. The micrographs of the ground powders showed that grain size distribution was not uniform. Improved connectivity of the grains was observed with the increasing of Ho_2O_3 doping. The micrograph of the sample contains almost fluently distributed and spherical shaped grains. The presence of voids of irregular dimensions indicates that the powders have a certain degree of porosity.

3.2. Thermal analysis

The DTA and TG curves of the $(Bi_2O_3)_{0.80}(Ho_2O_3)_{0.15}(Tm_2O_3)_{0.05}$ sample represented by blue and red lines, respectively, are given in Fig. 4. The TG curve shows the weight loss of the sample during the thermal treatment process. As seen from the TG curve, there is almost no mass loss during the heating and cooling process. This means that the sample is stable at all temperatures. On the other hand, neither endothermic peaks nor exothermic peaks are seen between 30 and 800 °C during the heating and cooling cycle. This shows that there is no phase transition during the heat treatment and the δ-phase is preserved and stable even at room temperature.

3.3. Thermo-electrical properties

The electrical conductivity log σ curves of the $(Bi_2O_3)_{1-x-y}(Ho_2O_3)_x(Tm_2O_3)_y$ ternary system for $x=15$ mol% Ho_2O_3 and $y=5$, 10, 15, 20 mol% Tm_2O_3 obtained at 750 °C for 100 h in air versus $1000/T(^\circ C)$ are given in Fig. 5. The electrical conductivity measurements were carried out from room temperature to just below the melting point of the circular-shaped pellet samples. As can be seen from Fig. 5, all the curves are coincident with each other. This is the expected result since all of them have the stable δ-phase.

The electrical conductivity log σ curves of the $(Bi_2O_3)_{1-x-y}(Ho_2O_3)_x(Tm_2O_3)_y$ ternary system for $x=20$ mol% Ho_2O_3 and $y=5$, 10, 15, 20 mol% Tm_2O_3 versus $1000/T(^\circ C)$ are given Fig. 6. The behavior of these curves is the same as the curves in Fig. 5.

Table 1
Doping amount, electrical conductivity, average crystallite size, activation energy and unit cell parameters of the samples annealed at 750 °C for 100 h.

Samples	Ho_2O_3 doping (x=mole%)	Tm_2O_3 doping (y=mole%)	Bi_2O_3 doping ($1-x-y$=mole%)	Electrical conductivity 850 °C$(\Omega\,cm)^{-1}$	Crystallite size (nm)	Activation energy (eV)	Unit cell parameter (Å)
A1	15	5	80	1.82×10^{-1}	68.10	0.76	5.494
A2	15	10	75	1.38×10^{-1}	62.20	0.77	5.491
A3	15	15	70	6.19×10^{-2}	46.10	0.76	5.482
A4	15	20	65	5.30×10^{-2}	34.10	0.77	5.455
B1	20	5	75	1.85×10^{-1}	119.10	0.75	5.496
B2	20	10	70	9.01×10^{-2}	89.30	0.78	5.477
B3	20	15	65	5.51×10^{-2}	52.90	0.86	5.460
B4	20	20	60	1.90×10^{-2}	33.20	1.01	5.441

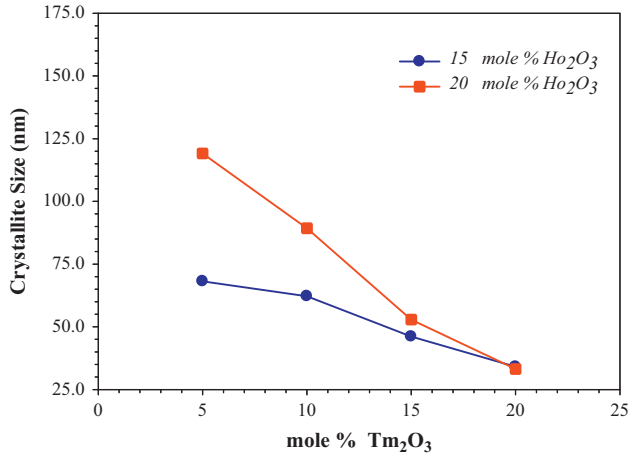

Fig. 2. The crystallite sizes of the materials as a function of Tm_2O_3 amount.

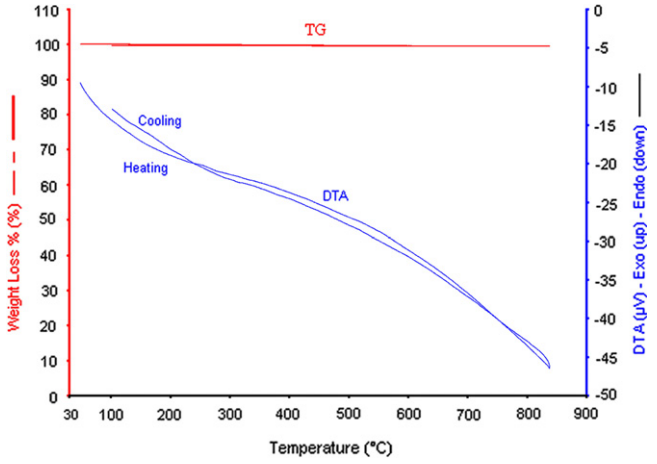

Fig. 4. DTA/TG curves of sample $(Bi_2O_3)_{0.80}(Ho_2O_3)_{0.15}(Tm_2O_3)_{0.05}$.

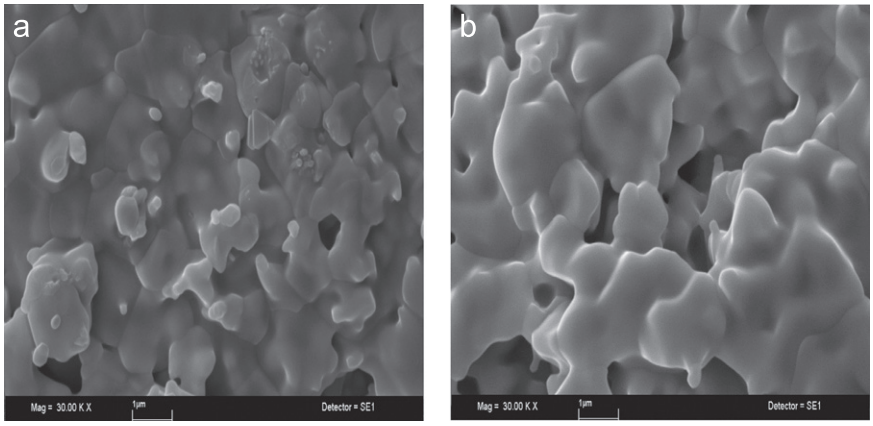

Fig. 3. The SEM micrograph for (a) $(Bi_2O_3)_{0.80}(Ho_2O_3)_{0.15}(Tm_2O_3)_{0.05}$ and (b) $(Bi_2O_3)_{0.75}(Ho_2O_3)_{0.20}(Tm_2O_3)_{0.05}$.

From Figs.5 and 6, it can be said that the Ho_2O_3 rich samples have higher electrical conductivity than the Tm_2O_3 rich ones. The electrical conductivity values of the samples corresponding to 850 °C are given in Table 1. It can be seen that the conductivity of the samples decreases slightly while the amount of Tm_2O_3 increases. This behavior can be attributed to the decrease in the proportion of highly polarizable cations and the number of oxide ion vacancies. The highest conductivity value of the sample (x=20 and y=5 mol%) is $5.31\times10^{-1}\,\Omega\,cm^{-1}$ at 1000 °C. This can be explained simply by the increase in the concentration of vacancies due to the Ho cations located on the host sublattice, which are available for oxide ion migration. The distribution of vacancies affects the long range migration

of oxide ions. Therefore, the conductivity of the sample increases.

The activation energies of the samples can be obtained from the Arrhenius equation. The temperature dependence of electrical conductivity σ also indicates that the electrical conduction in the ceramic material is governed bythe Arrhenius relation

$$\boldsymbol{\sigma} = \sigma_0 \exp\left(-E_a/k_B T\right) \tag{3}$$

where σ_0 denotes the pre-exponential factors, E_a is the activation energies of the mobile ions, k_B is the Boltzmann's constant and T is the temperature in Kelvin. The calculated activation energies of the samples are given in Table 1.

The activation energy values of the $(Bi_2O_3)_{1-x-y}(Ho_2O_3)_x(Tm_2O_3)_y$ ternary systems for $x=15$ mol% Ho_2O_3 and $y=5$, 10, 15, 20 mol% Tm_2O_3 and for $x=20$ mol% Ho_2O_3 and $y=5$, 10, 15, 20 mol% Tm_2O_3 synthesized at 750 °C for 100 h in air were calculated. The activation energy curves of these two samples versus amount of dopant of Tm_2O_3 obtained using the calculated activation energy values are seen in Fig. 7. The activation energy results are also given in Table 1. For the samples with $x=15$ mole% Ho_2O_3 and $y=5$, 10, 15, 20 mol% Tm_2O_3, the activation energies of the samples are almost the same and do not change with the amount of Tm_2O_3. However, the activation energies of the second samples with $x=20$ mol% Ho_2O_3 increase by increasing the doping amount of Tm_2O_3. This result shows that the electrical conductivity of the samples decreases with mol% Tm_2O_3. As expected, the sample with high activation energy has low electrical conductivity. This can be seen in Table 1. Since the dopant cations and oxide ion vacancies have negative and positive charges, the attractions between them are likely to be mainly responsible for the value of the activation energy. The samples which exhibit the lowest activation energy associated with the structure characterized by the fluorite type fcc lattice are likely to be responsible for the opening of migration pathways for the oxide ions, and consequently to a decrease in the activation energy (Fig. 7).

The low temperature conductivity results (below 300 °C) were not taken into consideration because of the poor conductivities of the studied samples.

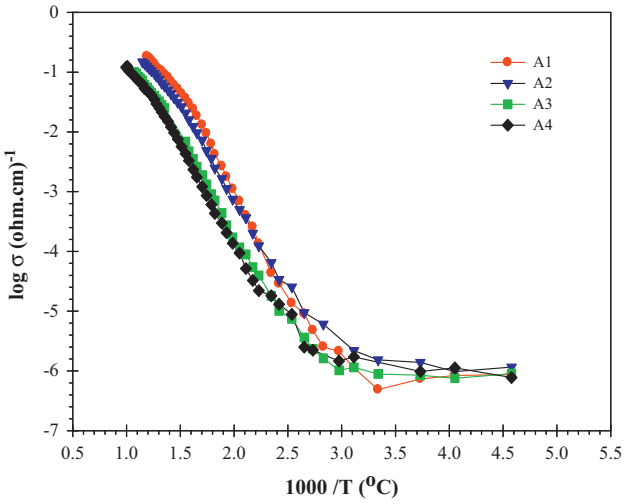

Fig. 5. The temperature dependence of total electrical conductivity (σ_T) for $x=15$ mol% Ho_2O_3 and $y=5$, 10, 15, 20 mol% Tm_2O_3 (given in Table 1).

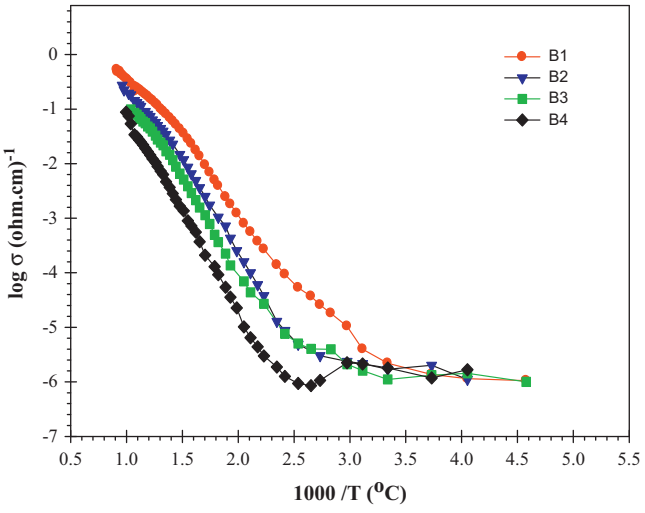

Fig. 6. The temperature dependence of total electrical conductivity (σ_T) for $x=20$ mol% Ho_2O_3 and $y=5$, 10, 15, 20 mol% Tm_2O_3 (given in Table 1).

4. Conclusions

In this work, $(Bi_2O_3)_{1-x-y}(Ho_2O_3)_x(Tm_2O_3)_y$ ($x=15$, 20 mol%, $y=5$, 10, 15, 20 mol%) ternary system materials synthesized by the solid state reaction method were investigated in detail and some important results were obtained from XRD, TG/DTA, and 4PPT experimental measurements. According to the XRD and DTA results all the samples have a dominantly homogeneous fluorite type fcc δ-Bi_2O_3 phase. The stable δ-phase of the $(Bi_2O_3)_{1-x-y}(Ho_2O_3)_x(Tm_2O_3)_y$

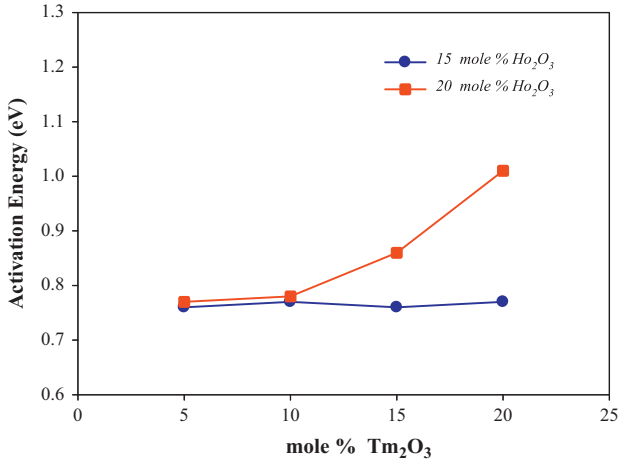

Fig. 7. The activation energies of the samples as a function of Tm_2O_3 doping amount.

ternary system does not change in the operation conditions of an SOFC. This property was observed for the first time in this study. According to the conductivity measurement results, all the samples have a high oxygen ion conductivity property. It was observed that the electrical conductivity of all the samples increase while the mole percentage of the Tm_2O_3 doping materials decrease. The best electrical conductivity was observed for the sample $(Bi_2O_3)_{0.75}(Ho_2O_3)_{0.20}(Tm_2O_3)_{0.05}$ synthesized at 750 °C for 100 h and the maximum conductivity value was measured as $5.31 \times 10^{-1}\,\Omega\,cm^{-1}$ at 1000 °C. This sample also has the lowest activation energy which is calculated by using the Arrhenius equation. As consequences of these results, we found that these materials can be used as electrolyte, especially in SOFCs, due to their high oxygen ion conductivity and structural stability properties.

Acknowledgements

The authors would like to thank Erciyes University's Research Fund for its financial supported (Project no: FBA-11-3525).

References

[1] N.Q. Minh, Ceramic fuel cells, Journal of the American Ceramic Society 76 (1993) 563–588.
[2] K.Z. Fung, H.D. Baek, A.V. Virkar, Thermodynamic and kinetic considerations for Bi_2O_3-based electrolytes, Solid State Ionics 52 (1992) 199–211.
[3] K. Traina, M.C. Steil, J.P. Pirard, C. Henrist, A. Rulmont, R. Cloots, B. Vertruyen, Synthesis of $La_{0.9}Sr_{0.1}Ga_{0.8}Mg_{0.2}O_{2.85}$ by successive freeze-drying and self-ignition of a hydroxypropylmethyl cellulose solution, Journal of the European Ceramic Society 27 (2007) 3469–3474.
[4] D. Hari Prasad, J.W. Son, B.K. Kim, H.W. Lee, J.H. Lee, Synthesis of nano-crystalline $Ce_{0.9}Gd_{0.1}O_{1.95}$ electrolyte by novel sol–gel thermolysis process for IT-SOFCs, Journal of the European Ceramic Society 28 (2008) 3107–3112.
[5] I.M. Hung, H.W. Peng, S.L. Zheng, C.P. Lin, J.S. Wu, Phase stability and conductivity of $Ba_{1-y}Sr_yCe_{1-x}Y_xO_{3-\delta}$ solid oxide fuel cell electrolyte, Journal of PowerSources 193 (2009) 155–159.
[6] N.M. Sammes, G.A. Tompsett, H. Näfe, F. Aldinger, Bismuth based oxide electrolytes structure and ionic conductivity, Journal of the European Ceramic Society 19 (1999) 1801–1826.
[7] J.C. Boivin, Structural and electrochemical features of fast oxide ion conductors, Journal of Inorganic Materials 3 (2001) 1261–1266.
[8] A. Basu, A.W. Brinkman, T. Hashemi, NTC characteristics of bismuth based ceramics at high temperature, Journal of Inorganic Materials 3 (2001) 1219–1221.
[9] T.P. Gujar, V.R. Shinde, C.D. Lokhande, R.S. Mane, S.H. Han, Bismuth oxide thin films prepared by chemical bath deposition (CBD) method: annealing effect, Applied Surface Science 250 (2005) 161–167.
[10] H.S. Cho, G. Sakai, K. Shimanoe, N. Yamazoe, Preparation of $BiMeVO_x$ (Me=Cu, Ti, Zr, Nb, Ta) compounds as solid electrolyte and behavior of their oxygen concentration cells, Sens. Actuators, B 109 (2005) 307–314.
[11] M.G. Stachiotti, R. Machado, A. Frattini, N. Pellegri, O.D. Sanctis, Effects of the chemical modifier on the thermal evolution of $SrBi_2Ta_2O_9$ precursor powders, Journal of Sol-Gel Science Technology 36 (2005) 53–60.
[12] K.R. Kendall, C. Navas, J.K. Thomas, H.C. Loye, Recent developments in perovskite-based oxide ion conductors, Solid State Ionics 82 (1995) 215–223.
[13] O. Labidi, M. Drache, P. Roussel, J.P. Wignacourt, Crystal structures and conductivity properties of $MBi_6V_2O_{15}$ family type compounds (M=Pb, Sr, Ca, Cd, $Na_{0.5}Bi_{0.5}$), Solid State Sciences 9 (2007) 964–972.
[14] M. Leszczynska, M. Holdynski, I. Abrahams, X. Lui, W. Wrobel, Structural and electrical properties of $Bi_3Nb_{1-x}Er_xO_{7-x}$, Solid State Ionics 181 (2010) 796–811.
[15] N.A.S. Webster, C.D. Ling, C.L. Raston, F.J. Lincoln, The structure and conductivity of new fluorite-type Bi_2O_3–Er_2O_3–PbO materials, Solid State Ionics 178 (2007) 1451–1457.
[16] J.Y. Park, H. Yoon, E.D. Wachsman, Fabrication and characterization of high-conductivity bilayer electrolytes for intermediate-temperature solid oxide fuel cells, Journal of the American Ceramic Society 2402 (2005) 88.
[17] Q. Zhen, G.M. Kale, W. He, J. Liu, Microwave plasma sintered nanocrystalline Bi_2O_3–HfO_2–Y_2O_3 composite solid electrolyte, Chemistry of Materials 19 (2007) 203–210.
[18] A. Watanabe, M. Sekita, Stabilized δ-Bi_2O_3 phase in the system Bi_2O_3–Er_2O_3–WO_3 and its oxide–ion conduction, Solid State Ionics 176 (2005) 2429–2433.
[19] D.W. Jung, J.C. Nino, K.L. Duncan, S.R. Bishop, E.D. Wachsman,Enhanced, Long-term stability of bismuth oxide-based electrolytes for operation at 500 °C, Ionics 16 (2010) 97–103.
[20] C.Y. Hsieh, K.Z. Fung, Crystal structure and electrical conductivity of cubic fluorite-based $(YO_{1.5})_x(WO_3)_{0.15}(BiO_{1.5})_{0.85-x}$ $(0 \le x \le 0.4)$ solid solutions, Journal of Solid State Electrochemistry 13 (2009) 951–957.
[21] M. Drache, P. Roussel, J.P. Wignacourt, Structures and oxide mobility in Bi–Ln–Omaterials: heritage of Bi_2O_3, Chemical Reviews 107 (2007) 80–86.
[22] G.H. Zhong, J.L. Wang, Z. Zeng, The doping effects in δ-Bi_2O_3 oxide ionic conductor, Physics. State.Solid. (b) 12 (2008) 2737–2742.
[23] S. Arasteh, A. Maghsoudipour, M. Alizadeh, A. Nemati, Effect of Y_2O_3 and Er_2O_3 co-dopants on phase stabilization of bismuth oxide, Ceramics International 37 (2011) 3451–3455.
[24] F. Krok, I. Abrahams, H. Holdynski, A. Kozanecka-Szmigiel, M. Malys, M. Struzik, X. Liu, J.R. Dygas, Oxide ion distribution and conductivity in $Bi_7Nb_{2-2x}Y_{2x}O_{15.5-2x}$, Solid State Ionics 179 (2008) 975–980.
[25] M. Yashima, D. Ishimura, Visualization of the diffusion path in the fast oxide-ion conductor $Bi_{1.4}Yb_{0.6}O_3$, Applied Physics Letter 87 (2005) 221909.